PHYSICAL REVIEW B VOLUME 15, NUMBER 8 15 APRIL 1977

Further evaluation of the transform-deconvolution method for surface-structure determination by analysis of low-energy electron-diffraction intensities

David L. Adams
Institute of Physics, University of Aarhus, DK 8000 Aarhus C, Denmark

Uzi Landman
Institute for Fundamental Studies, Department of Physics and Astronomy, University of Rochester, Rochester, New York 14627

(Received 23 August 1976)

The conventional approach to surface structure determination by analysis of low-energy electron diffraction (LEED) consists of comparison between experimental intensities and intensities calculated on the basis of a model of the diffraction process and a trial model of the surface structure. Although this model calculation approach has been used with some success in the case of simple structures, it is unlikely that it can be easily extended to more complex systems unless a reasonable approximation to the structure is known or can be determined by another method. In this article we further describe and evaluate the transform-deconvolution method, which is in essence an adaption to LEED of the Patterson function method of x-ray crystallography, in which direct use is made of the experimental data without prior assumption of a model structure. Within the approximation of single-scattering theory it is shown that the Patterson functions of LEED intensities consist of sums of convolution products of structural and nonstructural terms from which the structural parameters can be recovered via a deconvolution process. Procedures are described for tackling the problem of nonuniqueness, which results from the limited amount of data available from a LEED experiment, and problems associated with the effects of multiple scattering. The results of application of the transform-deconvolution method to the analysis of LEED intensities from Cu(100), Ni(100), Al(111), and Al(100) are presented. Consistent values for the surface interlayer spacings are obtained from the analysis of a number of intensity spectra in each case.

I. INTRODUCTION

In the last decade the introduction of a wide variety of new experimental techniques has greatly extended the capability for obtaining detailed information concerning surface properties and adsorption phenomena.[1,2] The recent use of ultraviolet and x-ray induced photoemission spectroscopies in well-controlled surface experiments[3,4] has led to a redirection of emphasis from atomistic to electronic properties. However, the present, general lack of accurate structural information is an impediment to a detailed understanding of the changes in electronic configuration caused by the presence of a surface or caused by the adsorption of foreign atoms.

Low-energy electron diffraction[5] (LEED) still appears to be the most likely method for accurate determination of surface structure. Recent model calculations of LEED intensities have shown encouraging signs of approaching agreement with experimental measurements in the case of some simple structures.[6,7] These improvements together with the use of perturbation schemes[7] for efficient description of multiple-scattering processes appear to indicate that the main ingredients of the theoretical treatment can now be handled in a fairly accurate and practical way.

The major drawback of the model-calculation approach, however, is the need to carry out an exhaustive search of parameter space in order to obtain best agreement between calculated and experimental LEED intensities. At the present time, the computational requirements of dynamic model calculations are too large to permit a proper variation over the model parameters analogous, for example, to least-squares refinement methods of x-ray crystallography. In addition, the comparison between experimental and calculated intensities is generally carried out in a rudimentary fashion and is made uncertain by the lack of well-defined criteria for assessing the extent of agreement. The general inability to perform a complete parameter variation inevitably brings into question the uniqueness of structure determination. This problem is compounded by the relative paucity of data available from a LEED experiment as compared to an x-ray diffraction study. Some of the conflicting structural interpretations which have appeared in the recent literature,[8,9] and which have been the source of some confusion and controversy, can be clearly attributed to the occurrence of false local maxima in (hypothetical) plots of "goodness of fit" in parameter space.

In the analogous case of bulk structure determination via x-ray diffraction, model calculations are

used in structural *refinement* after good approximations to the structure have been found using one of the direct methods of analysis, which are based on inversion of the experimental data without prior assumption of a structural model. It seems to us quite evident that extension of LEED analysis to more complex surface structures is unlikely to be of wide use unless analogous direct methods can be similarly applied to yield first approximations to the surface structure.

In recent papers,[10–14] we have described the principles of a direct method for analysis of LEED intensities which is related to the Patterson[15] function method of x-ray crystallography. As in the x-ray case, the method takes a more approximate view of the diffraction process than can be achieved in a dynamic model calculation. Nevertheless, it will be argued on the basis of analysis of experimental data that the method is in fact capable of yielding a good approximation to the surface structure.

In Sec. II we discuss the Patterson functions of LEED intensities and show that these contain sums of convolution products of structural and nonstructural terms. In Sec. III, the transform-deconvolution method for retrieval of structural information from the Patterson functions is reviewed, together with a more detailed account of its practical implementation than has been given hitherto, including important new refinements. Application of the method to the analysis of experimental LEED data for Cu(100), Ni(100), Al(111), and Al(100) is presented in Sec. IV. The extension of the method to the analysis of overlayer systems is discussed in Sec. V. Finally, conclusions and future directions are considered in Sec. VI.

II. PATTERSON FUNCTIONS OF LEED INTENSITIES

In the case of x-ray crystallography, the Patterson function is obtained by Fourier inversion of the diffracted intensities[15,16]

$$P(xyz)=\sum_h\sum_k\sum_l I_{hkl}\,e^{-2\pi i(hx+ky+lz)}, \tag{2.1}$$

where I_{hkl} is the intensity of the hkl reflection. In the absence of anomalous dispersion, Friedel's law, $I_{hkl}=I_{\bar{h}\bar{k}\bar{l}}$, applies and so Eq. (2.1) reduces to a cosine transform and $P(xyz)$ is therefore a real, even function. In the case of single-scattering it has been shown[15] that $P(xyz)$ is given by the self-convolution of the real-space scattering potential. Thus peaks are found in $P(xyz)$ at positions determined by all interatomic vectors within the unit cell; the vectors being translated to a common origin. The real-space structure is obtained by forming the convolution square root of $P(xyz)$.[16]

In the case of LEED, the third Laue condition is not properly established due to the strong inelastic scattering of low-energy electrons in solids. The intensity of an hk *beam* varies continuously along the l direction of reciprocal space, corresponding to the surface normal direction. Thus Eq. (2.1) must be rewritten as

$$P(xyz)=\sum_h\sum_k\left(\int I_{hk}(s)e^{-2\pi isz}\,ds\right)e^{-2\pi i(hx+ky)}, \tag{2.2}$$

where $2\pi s$ is the normal component of the diffracted wave vector. Friedel's law does not apply, so $P(xyz)$ is, in general, complex.[17]

As we have discussed previously,[10–14] reduced forms of the three-dimensional Patterson function $P(xyz)$ can be conveniently used in the analysis of LEED intensities. In this article we focus upon the use of the one-dimensional line projection $P(z)$, which in the x-ray case contains peaks at positions corresponding to all interatomic vectors projected on to the z axis and translated to a common origin. In the case of LEED, $P(z)$ is given by

$$P(z)=\int I_{00}(s)\,e^{-2\pi isz}\,ds, \tag{2.3}$$

where z is the surface normal direction and $I_{00}(s)$ is the intensity of the specular diffracted beam. From considerations of symmetry[17] $I_{00}(s)=I_{00}(-s)$ and therefore $P(z)$ is obtained as a real, even function given by

$$P(z)=2\int I_{00}(s)\cos 2\pi sz\,ds. \tag{2.4}$$

The physical significance of the $P(z)$ function obtained by Fourier inversion of specular-beam LEED intensities has been discussed on the basis of analytical Fourier transformation of expressions for both kinematic single-scattering intensities,[11–14] and for dynamic multiple-scattering intensities.[18] In the following we briefly reproduce the derivation for the case of kinematic intensities since this result forms the basis for the transform-deconvolution method. The additional consequences of multiple scattering are considered later.

We take as a model structure the case of an adsorbed layer with scattering factor $f_0(s)$, taken to be renormalized with respect to adsorbate coverage, at a distance d_0 above the outermost plane of the substrate. The substrate scattering factor is $f_s(s)$ and the uniform interlayer spacing in the substrate is d_s. The atomic scattering factors are taken to be renormalized with respect to thermal vibrations by multiplication of the rigid-lattice scattering factors by a Debye-Waller factor. Attenuation of the electron beam inside the solid

by inelastic processes and by destructive interference with elastically scattered electrons is simulated by assuming an energy-independent layer attenuation exponent μ. Defining attenuation factors $\alpha_0 = e^{-\mu d_0/\cos\theta}$ and $\alpha_s = e^{-\mu d_s/\cos\theta}$ where θ is the angle of incidence, and defining phase angles $\beta_0 = 2\pi s d_0$ and $\beta_s = 2\pi s d_s$, then the diffracted intensity in the specular beam can be written in terms of a sum over the amplitudes scattered from each layer

$$I_{00}(s) = \left| f_0(s) + f_s(s)\alpha_0 \sum_{\nu=0}^{\infty} \alpha_s^{\nu} e^{i(\beta_0 + \nu\beta_s)} \right|^2$$

$$= f_0(s) f_0^*(s) + f_s^*(s) f_s(s) \alpha_0^2 (1 - \alpha_s^2)^{-1}$$

$$\times \sum_{\nu=0}^{\infty} \alpha_s^{\nu} (e^{i\nu\beta_s} + \epsilon^{-i\nu\beta_s} - 1) + \alpha_0 \sum_{\nu=0}^{\infty} \alpha_s^{\nu} [f_0(s) f_s^*(s) e^{-i(\beta_0 + \nu\beta_s)} + f_s(s) f_0^*(s) e^{i(\beta_0 + \nu\beta_s)}], \tag{2.5}$$

where the asterisk indicates complex conjugate.

Ignoring for the moment the fact that experimental intensities are available only for a truncated range of s, Fourier transformation of $I_{00}(s)$ according to Eq. (2.4) yields

$$P(z) = P_0(z) * F_{00}(z) + \alpha_0^2 P_s(z) * F_{ss}(z) + P_{s0}(z) * F_{s0}(z) + P_{0s}(z) * F_{0s}(z), \tag{2.6}$$

where $*$ denotes the convolution operation. $P_0(z)$, $P_s(z)$, $P_{s0}(z)$, and $P_{0s}(z)$ are given by

$$P_0(z) = \delta(z),$$

$$P_s(z) = (1 - \alpha_s^2)^{-1} \sum_{\nu=0}^{\infty} \alpha_s^{\nu} [\delta(z - \nu d_s) + \delta(z + \nu d_s) - \delta(z)], \tag{2.7}$$

$$P_{s0}(z) = \alpha_0 \sum_{\nu=0}^{\infty} \alpha_s^{\nu} \delta(z + d_0 + \nu d_s),$$

$$P_{0s}(z) = \alpha_0 \sum_{\nu=0}^{\infty} \alpha_s^{\nu} \delta(z - d_0 - \nu d_s),$$

where $\delta(x)$ is the Dirac delta function. $F_{00}(z)$, $F_{ss}(z)$, $F_{s0}(z)$, and $F_{0s}(z)$ are, respectively, the Fourier cosine transforms of $f_0(s)f_0^*(s)$, $f_s(s)f_s^*(s)$, $f_s^*(s)f_0(s)$, and $f_0^*(s)f_s(s)$.

Two particular cases may be obtained from Eq. (2.6). For a clean substrate with first layer spacing d_0 different from subsequent spacings d_s,

$$P(z) = [P_0(z) + \alpha_0^2 P_s(z) + P_{s0}(z) + P_{0s}(z)] * F_{ss}(z). \tag{2.8}$$

For a clean substrate with uniform layer spacing d_s,

$$P(z) = P_s(z) * F_{ss}(z). \tag{2.9}$$

Thus in this last most-simple case the $P(z)$ function consists of a single set of δ functions positioned at multiples of the interlayer spacing d_s, convoluted with the Fourier transform of the modulus of the atomic scattering factor. The δ function amplitudes decay exponentially with increasing $|z|$ due to the factor α_s^{ν} associated with the attenuation of the incident and diffracted beams in the crystal.

In the analysis given above it has been assumed that $I_{00}(s)$ is known for all s. In a LEED experiment, however, the accessible range of s is limited to positive values and in practice is further truncated. This truncation has crucial consequences as discussed below.

The minimum (positive) value of s is defined by the inner potential of the solid as $s_1 = (1/\pi)(2m/\hbar)^{1/2} V_0^{1/2}$, since electrons incident upon the solid at zero energy increase in energy by V_0 upon entering the solid. In practice, s_1 is usually larger than the value given above because of the difficulty in working with electron beams of energy less than about 10 eV. The maximum value of s, s_2 is usually chosen arbitrarily by the experimentalist, but in general, the choice is very much influenced by the strong attenuation of diffracted intensity with increasing s due to the decrease in scattering factor, and by the desire to retain sensitivity to the surface layers.

Thus in practice the Fourier integral of Eq. (2.4) is truncated

$$P_T(z) = 2 \int_{s_1}^{s_2} I_{00}(s) \cos 2\pi s z \, ds. \tag{2.10}$$

Defining a box-car window ω_B according to

$$\omega_B(s) = \begin{cases} 1, & s_1 \leq |s| \leq s_2, \\ 0, & \text{elsewhere}, \end{cases} \tag{2.11}$$

then Eq. (2.10) can be written

$$P_T(z) = 2 \int_0^{\infty} \omega_B(s) I_{00}(s) \cos 2\pi s z \, ds. \tag{2.12}$$

Application of the convolution theorem to Eq. (2.12)

yields

$$P_T(z) = \left(2\int_{s_1}^{s_2} \cos 2\pi s z\, ds\right) * \left(2\int_0^{\infty} I_{00}(s)\cos 2\pi s z\, ds\right),$$

i.e.,

$$P_T(z) = W_B(z) * P(z), \tag{2.13}$$

where

$$W_B(z) = 2\int_{s_1}^{s_2} \cos 2\pi s z\, ds = \frac{\sin 2\pi s_2 z - \sin 2\pi s_1 z}{\pi z}. \tag{2.14}$$

Thus the expressions for $P(z)$ given in Eq. (2.6), (2.8), and (2.9) must be convoluted with $W_B(z)$ in the case of a truncated range of s. The equations can be applied directly if the Fourier transforms of the scattering factors are understood to be truncated, for example,

$$F_{ss}(z) = 2\int_{s_1}^{s_2} f_s(s) f_s^*(s)\cos 2\pi s z\, ds\,. \tag{2.15}$$

The equivalent derivation of $P(z)$ by Fourier transformation of $I_{00}(s)$, or by convolution of a set of delta functions $P_s(z)$ with the truncated Fourier transform $F_{ss}(z)$ of an atomic scattering factor is illustrated in Fig. 1 for the case of a clean substrate with uniform layer spacing.

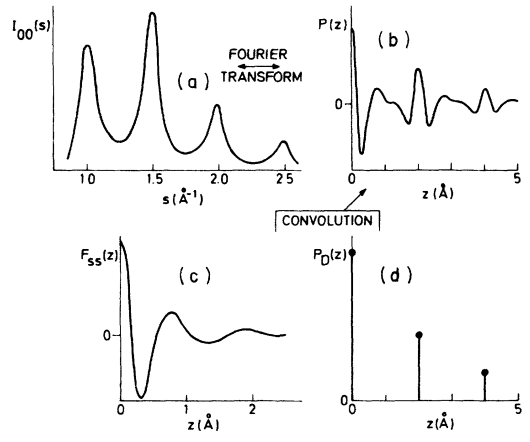

FIG. 1. Fourier transformation of calculated single-scattering intensities for the specular diffracted beam from a clean, uniform substrate and, equivalently, formation of $P(z)$ by convolution of a set of delta functions at multiples of the interlayer spacing with the truncated Fourier transform of an atomic scattering factor. Parameter values used in the calculations were appropriate for Al (100). (a) $I_{00}(s)$, calculated intensity spectrum. (b) $P(z)$, Fourier transform of (a). (c) $F_{ss}(z)$. (d) δ-function set.

III. TRANSFORM-DECONVOLUTION METHOD

As described in Sec. II, in the single-scattering approximation the Fourier transform $P(z)$ of specular-beam intensities contains convolution products of functions of the required structural parameters with truncated Fourier transforms of atomic scattering factors. The aim of the transform-deconvolution method is to perform a deconvolution of the structural and nonstructural content of $P(z)$.

Several difficult problems must be overcome in carrying out the deconvolution. In the case of a one-component system (clean substrate), for which in single-scattering theory the structural and nonstructural variables are separable, the major problem is the absence of a unique mathematical solution to the convolution equation owing to the truncation of the data. This problem is intensified by the additional effects of multiple scattering in mixing the variables. In the case of a multicomponent system (e.g., substrate plus overlayer), the structural and nonstructural variables in general are not separable so a unique mathematical solution would not exist even in the absence of truncation.

In the following, procedures for tackling the above-mentioned difficulties are described. The simpler case of a one-component system is considered first. Modifications and further approximations which are required for the case of a multicomponent system are discussed in Sec. V.

For a clean substrate, allowing for the possibility of expansion or contraction of the interlayer spacings near the surface, Eq. (2.8) can be generalized as

$$P(z) = P_D(z) * F_{ss}(z), \tag{3.1}$$

where $P_D(z)$ contains sets of delta functions associated with each different interlayer spacing. Given a knowledge of the inner potential $V_0(s)$, $P(z)$ is obtained by Fourier cosine transformation of a specular-beam intensity spectrum. $F_{ss}(z)$ is the correspondingly truncated cosine transform of the modulus of the atomic scattering factor $f_s(s)$. The rigid-lattice scattering factor $f_s^{\mathrm{RL}}(s)$ can be obtained from the partial-wave expansion

$$f_s^{\mathrm{RL}}(s) = \left| \frac{-i\cos\theta}{2\pi s} \sum_{l=0}^{\infty} (2l+1)(e^{2i\delta_l} - 1) P_l(\cos\Phi) \right|^2, \tag{3.2}$$

where δ_l is the lth partial-wave phase shift obtained by integration of the radial Schrödinger equation, using a model potential. In the equation, θ is the angle of incidence, Φ is the diffracted angle, and $P_l(\cos\Phi)$ is the lth Legendre polynominal. To a first approximation the effect of thermal vibrations can be included by multiplying the rigid-lat-

tice scattering factor $f_s^{RL}(s)$ by a Debye-Waller factor

$$f_s(s)=f_s^{RL}(s)\,e^{-\gamma(s)s^2}, \tag{3.3}$$

where

$$\gamma(s)=\frac{3h^2}{2Mk_B\Theta_D}\left[\frac{1}{4}+\left(\frac{T}{\Theta_D}\right)^2\int_0^{\Theta_D}\frac{x}{e^x-1}dx\right] \tag{3.4}$$

and Θ_D is an effective Debye temperature.

Thus ignoring for the moment any consequence of multiple scattering and any uncertainties in $V_0(s)$ and $f_s(s)$, determination of interlayer spacings requires solution of Eq. (3.1) for $P_D(z)$ given $P(z)$ and $F_{ss}(z)$. Unfortunately, as indicated above, a unique solution of Eq. (3.1) requires a knowledge of $I_{00}(s)$ for all s. There are therefore an infinite number of possible solutions for $P_D(z)$ since an infinite number of functions can be constructed equal to $I_{00}(s)$ in the measured range but arbitrarily different outside that range.

The problem of nonuniqueness in the interpretation of limited experimental data is rather common. It is evident that selection of the correct physical solution in such a situation requires that the solution algorithm be constrained by incorporation of *a priori* known information.

The main feature of the correct physical solution, $P_D(z)$, in the single-scattering approximation is that it contains vector sets of δ functions, as derived in the previous section. Thus in our first attempt[10] to implement the transform-deconvolution approach for experimental data analysis, for clean Ni(100), the procedure adopted was to convolute trial sets of δ functions with $F_{ss}(z)$ according to Eq. (3.1) and compare the results with the experimental transform $P(z)$. Reasonable correspondence was achieved between experimental and calculated $P(z)$ functions for a single set of δ functions at positions close to the bulk interlayer spacing in Ni(100), indicating that the effects of multiple scattering in the experimental intensities did not interfere too severely with the analysis. It was evident, however, that manual variation of the parameters characterizing the sets of δ functions, and visual comparison of the experimental and calculated $P(z)$ functions would be an inadequate procedure in the case of more complicated systems. In addition, in this first work the atomic scattering factor was crudely described using s-wave phase shifts only.

In more recent papers,[11-13] concerned with the analysis of experimental data for Al(100), a deconvolution procedure based on a relaxation method attributed to Southwell[19,20] was used to directly solve Eq. (3.1) for $P_D(z)$. Although the procedure does not involve prior assumptions concerning the general nature of $P_D(z)$, its construction is such that fortuitously it usually leads to solutions of the required form. In particular, it always correctly produces a solution whose maximum component is a delta function at the origin [see Eqs. (2.6)–(2.9)].

In general, however, the absence of built-in constraints in the Southwell method means that the problem of nonuniqueness is not sufficiently addressed. Therefore in the analysis of experimental data given in the following section we have used a new deconvolution scheme which in essence combines our two previous approaches. As the Southwell method constitutes a first step in the refined procedure it is convenient to briefly outline its essential features. A more detailed account is given elsewhere.[14]

With the functions evaluated on a discrete grid of z, Eq. (3.1) represents a system of linear equations. The Southwell method is an iterative relaxation scheme, for solution of such a system, in which the solution vector is obtained by adjusting the value of one component only in each iteration. A vector of residuals is defined by

$$P_{RES}(z)=P(z)-P_D(z)*F_{ss}(z). \tag{3.5}$$

The solution $P_D(z)$ is obtained by iterative reduction of the residuals

$$\begin{aligned}&\text{0th iteration: } P_{RES}^{(0)}=P(z);\ P_D^{(0)}(z)=0\\&\nu\text{th iteration: } P_{RES}^{(\nu)}=P_{RES}^{(\nu-1)}(z)-\Delta p(z')*F_{ss}(z);\\&\qquad\qquad P_D^{(\nu)}(z)=P_D^{(\nu-1)}(z)+\Delta p(z').\end{aligned} \tag{3.6}$$

In the νth iteration, the component of $P_D^{(\nu-1)}(z)$ to be adjusted is determined by the position z' of the maximum component of $P_{RES}^{(\nu-1)}(z)$. The amplitude $\Delta p(z')$ of the adjustment is then determined from the approximation

$$P_{RES}^{(\nu-1)}(z)\cong\Delta p(z')F_{ss}(0), \tag{3.7}$$

which amounts to taking the dominant term only of the discrete representation of the convolution integral of Eq. (3.1).

The progress of the Southwell scheme is illustrated in Fig. 2, based on the $P(z)$ function formed from calculated single-scattering intensities for a clean substrate consisting of unit scatterers with uniform interlayer spacing. For the case of unit scatterers $F_{ss}(z)$ is equal to $W_B(z)$, the $\sin x/x$ function given by Eq. (2.14). As shown in the figure, in the first iteration the truncation oscillations associated with the origin peak of $P_D(z)$ are removed from the residual. Accordingly, the possibility of correctly locating the next delta function of $P_D(z)$ is much enhanced.

In our previous applications[11-13] of the Southwell method it was found that deconvolutions of $P(z)$ functions of experimental intensities contained consistent vector sets of delta functions, which

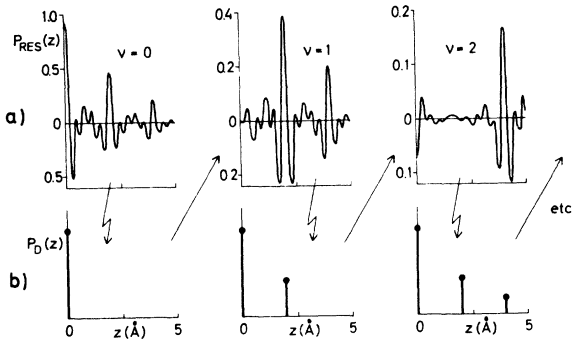

FIG. 2. Illustration of Southwell deconvolution scheme, using $P(z)$ function of calculated intensities from a uniform, point lattice with layer spacing 2 Å. In the zeroth iteration the residual function $P_{RES}(z)$ is set equal to $P(z)$. The maximum value of $P^{(0)}_{RES}(z)$ occurs at $z=0$, so a δ function is placed at the origin in the solution $P^{(1)}_D(z)$, with amplitude $P^{(0)}_{RES}(z)/F_{ss}(0)$. Convolution of $P^{(1)}_D(z)$ with $F_{ss}(z)$ and subtraction from $P^{(0)}_{RES}(z)$ yields $P^{(1)}_{RES}(z)$. The maximum value of $P^{(1)}_{RES}(z)$ occurs at $z=2$ Å so a δ function of amplitude $P^{(1)}_{RES}(2.0)/F_{ss}(0)$ is placed at this position in $P^{(2)}_D(z)$, and so on.

could be related to the surface structure, together with apparently random noise peaks. It was concluded that the noise peaks could probably be attributed, at least in part, to errors in description of the atomic scattering factor and thermal vibrations. A disadvantage of the procedure was that "signal" and "noise" peaks could not always be unambiguously distinguished, thereby creating some uncertainty in attempts to maximize signal to noise by variation of the values of the inner potential and Debye temperature used in the analysis. A related, practical difficulty was the need to carry out the analysis on a discrete grid of z.

In the light of our experience in applying the Southwell method we have evolved a considerably refined procedure described below. The main features are as follows:

(i). The convolution equation [Eq. (3.1)] is modified to explicitly account for the occurrence of errors in the input to the analysis and in a rough way to simulate the effects[18] of multiple scattering by including a noise component $P_N(z)$ in the solution

$$P(z)=[P_D(z)+P_N(z)]*F_{ss}(z)\,. \tag{3.8}$$

(ii). The solution algorithm is constrained to produce vector sets of delta functions, $P_D(z)$, and random noise, $P_N(z)$, which are unambiguously distinguished.

(iii). The interlayer spacings are no longer constrained to fall on a discrete grid.

(iv). A variation over the inner potential and an effective Debye temperature is carried out to maximize signal to noise in the deconvolution. The output values of V_0 and Θ_D are constrained to lie within physical bounds.

The main points of an algorithm incorporating these features are listed below:

(i). After addition of a first guess for V_0 to the energy scale, the experimental intensities are interpolated on to a uniform grid of s typically 0.02 Å^{-1}. $P(z)$ is then obtained, by numerical Fourier transformation of the intensities, on a uniform grid of z, with increment typically 0.05 Å and range 0–10 Å. $F_{ss}(z)$ is obtained by Fourier transformation, over the same range of s as the intensities, of a calculated scattering factor which includes a first guess for Θ_D. The scattering factor itself is typically calculated using 14 phase shifts derived from a model potential for the atomic species in question.

(ii). The Southwell deconvolution scheme is used, but is terminated after the first 2–4 iterations, yielding first approximations to the interlayer spacings, $d_i^{(0)}$; to the layer attenuation exponent $\mu^{(0)}$, calculated using the relative amplitudes of the delta functions; and to a scaling constant $c^{(0)}$.

(iii). Based on d_i, μ, and c, a *complete* $P_D(z)$ function is constructed using the analytical forms given in Eq. (2.6)–(2.9). $P_D(z)$ is convoluted with $F_{ss}(z)$ to give

$$P^{(\nu)}_{\text{calc}}(z)=[P^{(\nu)}_D(z)+P^{(\nu)}_N(z)]*F_{ss}(z)\,, \tag{3.9}$$

where $P_N(z)$ is an arbitrary function constructed on a uniform grid of z, with increment typically 0.1 Å and range 0–10 Å. $P_N(z)=0$ for all z in the zeroth iteration.

(iv). The $P(z)$ function derived from the experimental intensities is compared to the calculated function via an error indicator

$$R^{(\nu)}=\sum\left|P(z)-P^{(\nu)}_{\text{calc}}(z)\right|\Big/\sum\left|P(z)\right|\,. \tag{3.10}$$

(v). Steps (iii) and (iv) are iterated with a variation over d_i, μ, c, and $P_N(z)$ until $R\leq 0.1\%$. The minimization of R is performed using a conjugate-gradient algorithm which provides the values of $d_i^{(\nu)}$, $\mu^{(\nu)}$, $c^{(\nu)}$, and $P^{(\nu)}_N(z)$ for the first and subsequent iterations. We emphasize that in the zeroth iteration, the values $d_i^{(0)}$, $\mu^{(0)}$, and $c^{(0)}$ are derived from the experimental data via the Southwell method with no *a priori* structural assumptions being made.

In practice, it is convenient to divide the variation procedure into two stages. Firstly, d_i, μ, and c alone are varied, with $P_N(z)=0$, until a minimum value of R is obtained (typically about 10%). The values of d_i are subject to continuous variation.

Accordingly, $F_{ss}(z)$ must be interpolated to an appropriate uniform grid of z, based on the values of d_i, in order to perform the convolution of Eq. (3.9) and obtain $P_{\text{calc}}(z)$ on the same grid as $P(z)$. In the second stage $P_N(z)$ is varied, but with no further variation over d_i, μ, and c. This second stage is arbitrarily terminated when $R \leq 0.1\%$, at which point $P_N(z)$ has for all practical purposes converged.

Typically the first and crucial stage of the variation procedure involves variation over three–five parameters depending upon the number of different values of d_i. Construction of the noise component in the second stage involves variation over 101 parameters for the typical grid of z referred to above.

(vi). Finally, steps (i)–(v) are iterated with an outer variation over V_0 and Θ_D until a maximum of signal to noise is obtained in the deconvolution.

In interpreting the results of step (ii), we have typically restricted consideration of the number of different interlayer spacings d_i to $i \leq 3$, which is justified in general by the limited penetration of low-energy electrons into solids. In practice, in a particular analysis of a given experimental intensity spectrum, it is convenient, although not essential, to definitely constrain the value of i. Thus the algorithm is constrained to produce a solution with a single interlayer spacing, or with first layer spacing different from subsequent uniform layer spacing, or so on. The results of different analyses based on these different, general structural models are evaluated in terms of resultant signal to noise.

The procedure outlined above is based on the

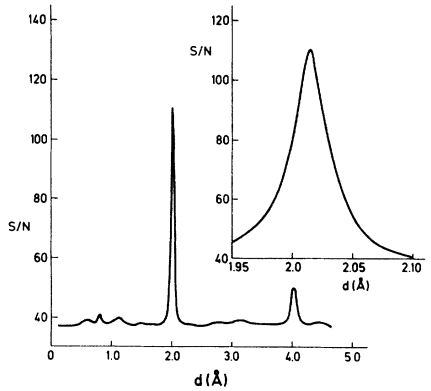

FIG. 3. Signal to noise vs d, the uniform interlayer spacing in the Al(100) surface. Plot constructed from many deconvolutions of the $P(z)$ function of an intensity spectrum for $\theta = 10°$, in which d was held fixed. All deconvolutions were carried out with fixed $V_0 = 16.6$ eV and $\Theta_D = 369$ °K. Inset shows the main peak at 2.01 Å on an expanded scale of z.

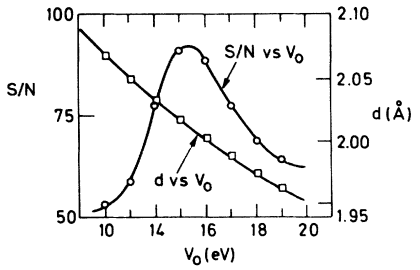

FIG. 4. Signal to noise vs V_0 for fixed $\Theta_D = 380$ °K. Variation of d with V_0 is also shown. Again based on data for Al(100), $\theta = 10°$.

proposition that errors in the input to the analysis and the effects of multiple scattering can be reasonably approximated by including a noise component in the deconvolution, and that the best approximation to the correct structural parameters is obtained from a deconvolution corresponding to a local maximum of signal to noise. Evaluation of the procedure must rest upon the results of experimental data analysis. For this reason we have concentrated to date upon the analysis of diffracted intensities from clean metal surfaces whose first interlayer spacings are believed, from the results of dynamic model calculations, to lie within ±10% of the bulk values. Apart from requiring sensible output values of the structural parameters, however, additional consistency checks can be applied. In particular, reasonable output values of the *nonstructural* parameters, V_0, Θ_D, and μ must be obtained. This criterion is used to discriminate between deconvolutions corresponding to different local maxima of signal to noise. In addition, analysis of intensity spectra taken for different angles of incidence and azimuth must produce internally self-consistent results.

Since the procedure involves a parameter variation to maximize signal to noise, S/N an obvious practical requirement is that plots of S/N versus both the structural and nonstructural parameters should exhibit well-defined maxima. To demonstrate that this is in fact the case, plots of S/N vs d, V_0, and Θ_D are shown in Figs. 3–5, respectively, from an analysis of an experimental intensity spectrum for Al(100). In these plots and in the analyses described in the following section, S/N was determined according to

$$\frac{S}{N} = P_D(0) \Big/ \sum |P_N(z)| \ . \tag{3.11}$$

The results were found to be essentially unaffected by the use of alternative measures of S/N, and the particular form used in Eq. (3.11) was chosen to avoid influence of the exponential decay of the δ

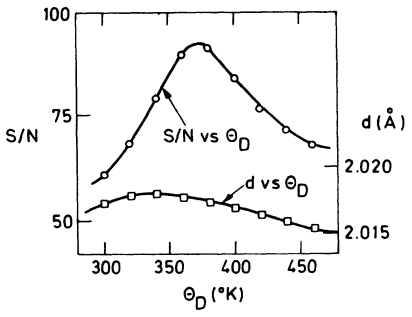

FIG. 5. Signal to noise vs Θ_D for fixed $V_0 = 16.0$ eV. Variation of d with Θ_D is also shown. Again obtained from deconvolutions of $P(z)$ function of Al(100), $\theta = 10°$ intensity spectrum.

function amplitudes upon the measure of signal weight.

In Fig. 3 is shown a plot of S/N vs d, for *fixed* V_0 and Θ_D, where d is the uniform interlayer spacing in the Al(100) surface (see below). The figure contains the results of a large number of deconvolutions, in each of which d was held fixed at a particular value. As can be seen from the figure, the result is not quite unambiguous since a small peak is found at 4.02 Å in addition to the dominant peak at 2.01 Å.

In this case it is evident that any well-designed variation procedure would converge to the correct result, but the fact that the first approximation obtained from the Southwell step of the deconvolution is $d = 2.05$ Å indicates the advantage of the Southwell step in accelerating convergence. In less favorable cases where competitive local maxima of signal to noise occur, the Southwell step is of critical importance in starting the solution in the vicinity of the physically meaningful local maximum.

In Fig. 4 is shown a plot of S/N vs V_0 for fixed Θ_D. The interlayer spacing d was allowed to vary in obtaining the deconvolutions used to construct this figure, and the corresponding plot of d vs V_0 is also shown. As can be seen, S/N exhibits a well-defined maximum as a function of V_0, although the dependence is weaker than upon d shown in Fig. 3. Nevertheless, the dependence of d upon V_0 shown in Fig. 4 indicates the need for an accurate choice of V_0 to obtain an accurate value of d.

A plot of S/N vs Θ_D for fixed V_0 is shown in Fig. 5. Again a well-defined maximum is obtained. The value of d was allowed to vary in the deconvolutions, but the plot of d vs Θ_D, also shown in the figure, indicates that d depends less critically upon Θ_D than upon V_0, as would be expected.

Thus it has been established that the signal-to-noise ratio in the deconvolution depends critically upon the value of the structural parameters and strongly upon the values of the nonstructural parameters, from which it appears that a variation procedure based on optimization of signal to noise should be viable.

It should also be noted that although the peak amplitudes and positions in plots of signal to noise, such as are shown in Fig. 3–5, depend upon the values assigned to the variables which are held fixed, the existence of well-defined maxima is not critical upon the assigned values. For example, the fixed values of Θ_D and V_0 used in constructing Figs. 4 and 5, respectively, are different from the optimum values, given in Table IV, which were obtained from an unrestricted deconvolution for the particular intensity spectrum considered here. It can be expected, therefore, that the variation procedure should be stable in the case of poorly chosen first guesses for V_0 and Θ_D.

IV. ANALYSIS OF EXPERIMENTAL DATA

In this section we present the results of applying the new version of the transform-deconvolution method to the analysis of experimental data for Cu(100),[21] Ni(100),[22] Al(111),[23] and Al(100).[11-13] In comparing the quality of the results obtained for these systems it should be noted that the accuracy of the input data varied widely. For Al(100) and Cu(100), an accurate representation of the original experimental data was available, in the former case from our work,[11-13] and in the case of Cu(100) through courtesy of Burkstrand[21] of General Motors. The data for Ni(100) and Al(111), however, were obtained from photographic enlargements of figures published in the literature, and hence were a less faithful representation of the original spectra.

We note that the energy ranges of the data used in the analysis were 15–260 eV for Cu(100), 15–240 eV for Ni(100), 10–200 eV for Al(111), and 10–240 eV for Al(100).

In the first analyses of the above systems, the deconvolution procedure was constrained to produce a *single* interlayer spacing. The propriety of this constraint is discussed later.

The results of the deconvolutions are summarized in Tables I–IV, which contain the output values for d, V_0, Θ_D, μ, and S/N for a number of different intensity spectra from each surface. Computer deconvolutions corresponding to the best and worst cases in terms of S/N for each system are shown in Figs. 6–9.

To a large extent the content of Tables I–IV and Figs. 6–9 is self-explanatory. Several points deserve emphasis, however. As can be seen from

TABLE I. Deconvolution output parameters for Cu(100).

θ (deg)	ϕ (deg)	d (Å)	V_0 (eV)	Θ (°K)	μ (Å^{-1})	S/N (arb)
10	0	1.81	12.0	181	0.24	59
10	5	1.81	11.8	180	0.25	62
10	10	1.80	13.0	198	0.32	65
10	45	1.78	10.0	190	0.57	50
12	0	1.81	12.0	170	0.32	57
12	10	1.81	12.0	176	0.40	54
12	45	1.78	12.1	195	0.49	47
a		1.80	11.9	184	0.36	
		±0.01	±0.8	±10	±0.11	

[a] Weighted mean values.

TABLE III. Deconvolution output parameters for Al(111).

θ (deg)	ϕ (deg)	d (Å)	V_0 (eV)	Θ_D (°K)	μ (Å^{-1})	S/N (arb)
10	0	2.25	18.0	322	0.43	86
15	0	2.27	14.8	360	0.42	72
20	0	2.25	17.0	310	0.40	73
25	0	2.25	20.8	338	0.51	85
10	30	2.27	16.0	327	0.43	95
15	30	2.26	18.0	369	0.42	79
20	30	2.31	16.0	325	0.38	87
25	30	2.31	20.9	350	0.44	59
a		2.27	17.6	337	0.43	
		±0.02	±2.0	±19	±0.04	

[a] Weighted mean values.

Figs. 6–9, even in the cases of worst signal to noise, the δ function signal is well distinguished from the noise. From Tables I–IV, it can be seen that analyses of different intensity spectra from the same surface gave very consistent values for the interlayer spacing d and for the inner potential V_0. The spread in output values of Θ_D and μ is generally higher, and systematic trends in the values of these parameters with angle of incidence occur in some cases. A completely consistent explanation for these trends cannot be found, but in the cases of Ni(100) and Al(100), for example, it is notable that Θ_D decreases with increasing angle of incidence. This behavior might be attributed to the increasing sensitivity to the outermost layers of the surface with their larger thermal vibrations.

The mean values of the output parameters for the four systems, weighted according to the signal to noise, are given in Table V, which also contains values of the bulk interlayer spacings, and the values of the volume-averaged inner potentials determined in the band-structure calculations of the crystal potentials[24,25] which were used to derive the scattering phase shifts. It can be seen from the table that for the (100) planes, the determined values of the surface interlayer spacing are within ±0.02 Å of the corresponding bulk spacings. The output values of the inner potentials are within ±1 eV of the calculated, volume-averaged values in the cases of Al(100), Al(111), and Cu(100). The output value for Ni(100) is 2 eV higher than the calculated value. Finally, the output values for Θ_D are generally similar to values used in model calculations for those systems,[21,26,27] and the values of the mean free path γ are consistent with experimental measurements.[28]

As mentioned previously, in the analyses described above the deconvolution procedure was constrained to produce a single interlayer spacing. In the case of the (100) planes, the results summarized in Table V indicate that this constraint was appropriate. In the case of Al(111), however, the mean value of d corresponds to a 3% contraction of the surface layer spacing relative to the bulk value.

TABLE II. Deconvolution output parameters for Ni(100).

θ (deg)	ϕ (deg)	d (Å)	V_0 (eV)	Θ_D (°K)	μ (Å^{-1})	S/N (arb)
6	0	1.77	16.0	328	0.69	54
8	0	1.79	14.1	284	0.43	56
10	0	1.78	16.0	320	0.32	61
12	0	1.79	15.9	280	0.24	70
14	0	1.78	15.8	246	0.34	56
a		1.78	15.6	291	0.39	
		±0.01	±0.7	±29	±0.15	

[a] Weighted mean values.

TABLE IV. Deconvolution output parameters for Al(100).

θ (deg)	ϕ (deg)	d (Å)	V_0 (eV)	Θ_D (°K)	μ (Å^{-1})	S/N (arb)
8	45	2.01	16.0	373	0.28	105
10	45	2.01	16.6	369	0.27	109
12	45	2.02	16.0	350	0.32	88
14	45	2.02	16.0	337	0.39	92
16	45	2.01	17.1	320	0.44	90
18	45	2.01	16.1	327	0.43	75
20	45	2.02	16.0	320	0.47	74
a		2.01	16.3	345	0.36	
		±0.01	±0.4	±21	±0.08	

[a] Weighted mean values.

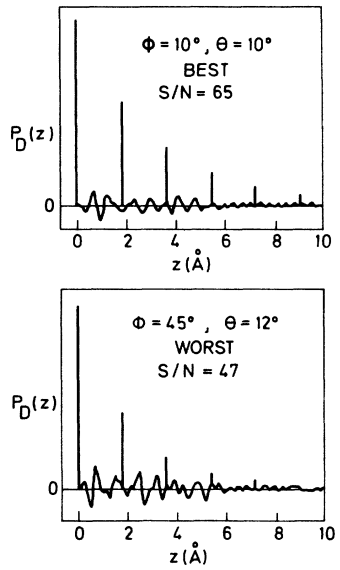

FIG. 6. Deconvolutions of $P(z)$ functions of intensity spectra for Cu(100), corresponding to the best and worst cases in terms of signal to noise of the seven intensity spectra which were analyzed (see Table I). The deconvolutions contain δ functions at multiples of the uniform interlayer spacing in the Cu(100) surface, together with a random noise component. The exponential decay of the δ-function series is due to the attenuation of the electron flux in the crystal, as characterized by the exponent μ.

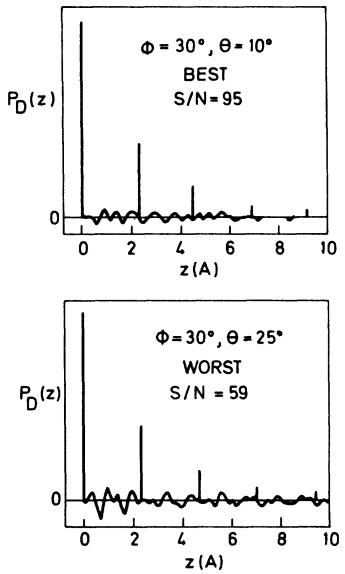

FIG. 8. Deconvolutions of $P(z)$ functions of intensity spectra for Al(111), corresponding to the best and worst cases in terms of signal to noise of the eight intensity spectra analyzed. For this surface the constraint of a uniform interlayer spacing is probably not justified since the derived value of 2.27 Å is ~ 3% less than the bulk value of 2.34 Å (see Table III and following text).

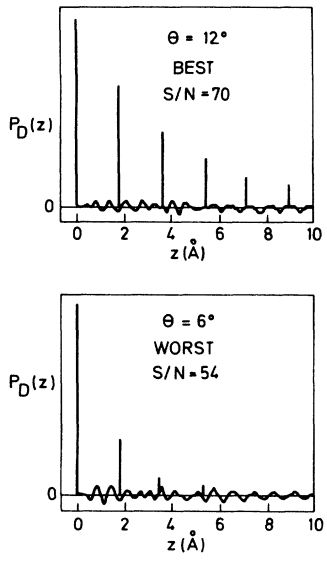

FIG. 7. Deconvolutions of $P(z)$ functions of intensity spectra for Ni(100), corresponding to the best and worst cases in terms of signal to noise of the five intensity spectra analyzed (see Table II).

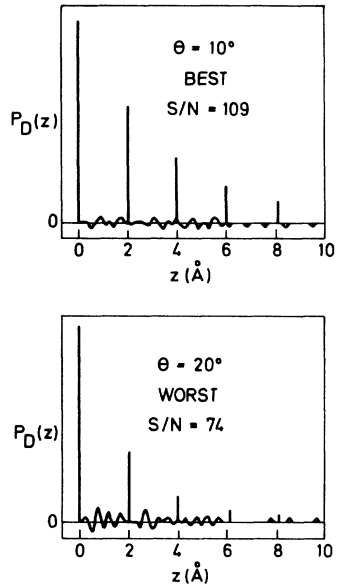

FIG. 9. Deconvolutions of $P(z)$ functions of intensity spectra for Al(100), corresponding to the best and worst cases in terms of signal to noise of the seven intensity spectra analyzed (see Table IV).

TABLE V. Mean values of output parameters.

Surface	d (Å)	V_0 (eV)	Θ_D (°K)	λ[a] (Å)	d_{Bulk} (Å)	V_{Inner} (eV)
Al(100)	2.01	16.3	345	5.6	2.025	16.7
Al(111)	2.27	17.6	337	4.7	2.34	16.7
Ni(100)	1.78	15.6	291	5.1	1.76	13.6
Cu(100)	1.80	11.9	184	5.6	1.81	12.4

[a]Mean free path $\lambda = 2/\mu$.

It is of interest therefore to determine if this contraction is genuine, or if it reflects systematic errors in the experimental data or the analysis. Accordingly the data for Al(111) and also, for the purpose of a consistency check, the data for (100) planes were reanalyzed with the deconvolution procedure constrained to produce a first interlayer spacing possibly *different* from subsequent spacings which were fixed at the bulk value. For this case the deconvolution contains two sets of delta functions, at $z = d_0 + \nu d_s$ and at $z = \nu d_s$, where d_0 is the first layer spacing.

A typical result for Al(111) is shown in Fig. 10. The value of the first layer spacing in this example is 2.24 Å compared to the value of 2.25 Å obtained previously (Table III) on the assumption of a uniform layer spacing. A complete analysis of the Al(111) intensity spectra confirmed this result; the mean value of the first layer spacing being 2.26 Å. However, the S/N values obtained in the second analysis were not significantly better than in the first. Also, the strong attenuation of the delta function amplitudes with increasing z led to less than unambiguous distinction between the νd_s set and the noise (see Fig. 10). Thus, while the second analysis of the Al(111) data does tend to confirm the occurrence of a contraction of the first layer spacing of 3%, it also indicates that resolution of differences in structural parameters of less than about 0.1 Å may be difficult of achieve without some ambiguity .

Finally, the reanalysis of the data for the (100) planes confirmed the result that the first layer spacing is within ±0.02 Å of the bulk value. A typical deconvolution is shown in Fig. 11 for Al(100). As shown in the figure, the two sets of delta functions are virtually coincident, although the value of the first layer spacing was allowed to vary freely. The values of S/N were essentially unchanged, as were the output values of V_0, Θ_D, and μ.

V. APPLICATION OF THE TRANSFORM-DECONVOLUTION METHOD TO OVERLAYER SYSTEMS

In this section we briefly consider the application of the transform-deconvolution method to the more difficult problem of systems containing more than one kind of surface atom.

For convenience, we consider the case of an adsorbed layer at a distance d_0 from the first layer of the substrate which has a uniform layer spacing d_s. This model contains the basic elements of a multicomponent system and can be discussed without loss of generality. The $P(z)$ function for this case is given by Eq. (2.6). As noted in Sec. II, the main difficulty in the analysis of multicomponent systems is the fact that even in single-scattering

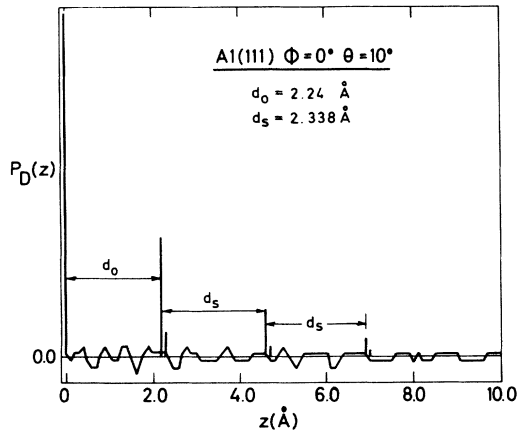

FIG. 10. Typical deconvolution of $P(z)$ function of an intensity spectrum for Al(111), in which the deconvolution was constrained to produce sets of δ functions at $z = \nu d_s$ and $z = d_0 + \nu d_s$. d_s was fixed at the bulk value of 2.338 Å, and the first layer spacing d_0 was allowed to vary freely.

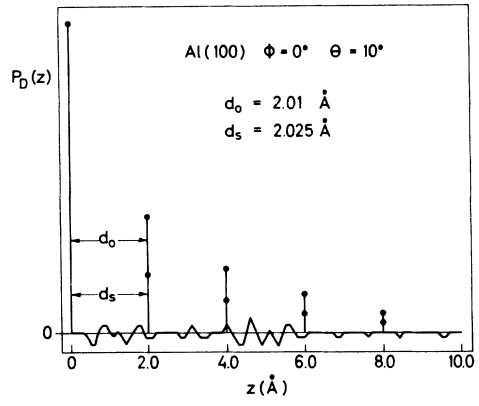

FIG. 11. Typical deconvolution of $P(z)$ function of an intensity spectrum for Al(100), in which the deconvolution was constrained to produce two sets of δ functions, as in the caption to Fig. 10, with d_s fixed at the bulk value of 2.025 Å.

theory the structural and nonstructural variables are not separable.

In a previous article[11] we suggested a means for achieving a separation of variables in the case where intensity spectra are measured for both a clean substrate and substrate plus overlayer. Defining the respective $P(z)$ functions as $P_{\mathrm{SUB}}(z)$ and $P_{\mathrm{OVER}}(z)$, then it was proposed[11] that a difference function $P_{\mathrm{DIFF}}(z)$ be formed by a weighted "substrate-subtraction" procedure

$$P_{\mathrm{DIFF}}(z) = P_{\mathrm{OVER}}(z) - \alpha_0^2 P_{\mathrm{SUB}}(z) - \delta(z) * F_{00}(z), \quad (5.1)$$

involving a variation over α_0^2. From Eqs. (2.6)–(2.9) it follows that

$$P_{\mathrm{DIFF}}(z) = P_{s0}(z) * F_{s0}(z) + P_{0s}(z) * F_{0s}(z), \quad (5.2)$$

and this equation can be solved for $P_{s0}(z)$ and $P_{0s}(z)$ using the procedure described in Sec. III.

While we expect that the substrate-subtraction procedure might be applicable in many cases, the necessary assumption that the substrate structure is unchanged upon adsorption cannot be expected to be generally valid. Thus a more general approach is required. The most promising approach appears to be a modification of the procedure outlined in Sec. III for one-component systems. The modification consists of making an approximate separation of variables by replacing the individual atomic scattering factors by an average scattering factor in the Southwell step of the procedure [see Eqs. (3.5)–(3.7)]. Having obtained a first approximation to the structural parameters in this manner, the individual scattering factors are used in the subsequent variational refinement procedure. To date this approach has been tested satisfactorily using calculated single scattering intensities, but has not yet been applied to experimental data analysis.

VI. CONCLUSIONS AND FUTURE DIRECTIONS

In this paper we have described further refinements and applications of the transform-deconvolution method for surface structure determination by analysis of LEED intensities. As we have indicated, the main advantages of the method are that it does not require prior assumption of a single specific model structure, and that it does not demand large computational requirements. These advantages are gained at the expense of an empirical treatment of multiple-scattering processes and, in the case of multicomponent systems, an approximate treatment of the atomic scattering factors in the first stage of the analysis. Additional approximations, which are also frequently made in dynamic model calculations, include the use of spherical model potentials in generating scattering phase shifts, the use of an energy-independent inner potential, and the description of thermal vibrations by means of a single Debye-Waller factor. We note that a more accurate treatment of these factors could be readily incorporated in the transform-deconvolution method if such a treatment were warranted.

In our judgement, the internal consistency of the analysis of experimental data for Cu(100), Ni(100), Al(111), and Al(100) presented in Sec. II suggests that the approximations mentioned above do not appear to lead to large systematic errors. We believe that these results for clean surfaces give grounds for some optimism as to the success of future applications to more complex systems.

At its present stage of development, the transform-deconvolution method applies only to the determination of interlayer spacings via analysis of Fourier transforms of intensity spectra for the specular diffracted beam. We believe, however, that its extension to the case of two-dimensional sections[10–14] for the purpose of determination of layer structure and registry should be quite straightforward. The additional problem of truncation of the Fourier sums over h and k in this latter case is defined by the extent of the experimental data, and should be soluble without the requirement of ancillary physical information concerning the system under study.

Finally, we should like to comment that the study of direct methods of analysis of LEED is a relatively new and largely unpopulated field. In this article we have argued that the development of rapid and economical direct methods, to at least provide a first approximation to surface structure determination for subsequent refinement via model calculations, is vital if the full potential of LEED is to be realized. In discussing the transform-deconvolution method in some detail we have hoped to show that the use of direct methods is feasible and thereby to encourage their further study and development.

ACKNOWLEDGMENTS

The authors wish to thank Inge Schmidt for her help in preparing the manuscript. The assistance of Svend Olesen, V. Blak Nielsen, and Tove Asmussen in constructing figures is also gratefully acknowledged.

[1]E. G. McRae and H. D. Hagstrum, in *Treatise on Solid-State Chemistry*, edited by N. B. Hannay (Plenum, New York, 1976), Vol. 6A, Chap. 2.
[2]T. N. Rhodin and D. L. Adams, in Ref. 1, Chap. 5.
[3]E. W. Plummer, in *Topics in Applied Physics*, edited by R. Gomer (Springer, Berlin, 1975).
[4]C. R. Brundle, in *Surface and Defect Properties of Solids* (The Chemical Society, London, 1972), Vol. 1, Chap. 6.
[5]C. J. Davisson and L. H. Germer, Nature 119, 558 (1927); Phys. Rev. 30, 705 (1927).
[6]J. E. Demuth, D. W. Jepsen, and P. M. Marcus, Phys. Rev. Lett. 31, 540 (1973); Solid State Commun. 13, 1311 (1973); Phys. Rev. Lett. 32, 1182 (1974).
[7]M. Van Hove and S. Y. Tong, J. Vac. Sci. Technol. 12, 230 (1975); Surf. Sci. 54, 91 (1976).
[8]T. N. Rhodin and S. Y. Tong, Phys. Today 28, 23 (1975).
[9]S. Andersson and J. B. Pendry, Solid State Commun. 16, 563 (1975).
[10]U. Landman and D. L. Adams, J. Vac. Sci. Technol. 11, 195 (1974).
[11]D. L. Adams and U. Landman, Phys. Rev. Lett. 33, 585 (1974).
[12]D. L. Adams, U. Landman, and J. C. Hamilton, J. Vac. Sci. Technol. 12, 206 (1975).
[13]U. Landman and D. L. Adams, Surf. Sci. 51, 149 (1975).
[14]D. L. Adams and U. Landman, in *Characterization of Metal Surfaces*, edited by L.-H. Lee (Academic, New York, 1977), pp. 211–270.
[15]A. L. Patterson, Phys. Rev. 46, 372 (1934).
[16]M. J. Buerger, *Vector Space* (Wiley, New York, 1959).
[17]Although Friedel's law is not applicable in the case of LEED, simplifications to the form of the Patterson function can be realized in some cases since from considerations of symmetry: $I_{hk}(s)=I_{hk}(-s)$. We are grateful to Michel van Hove for useful discussions on this point.
[18]U. Landman, Discuss. Faraday. Soc. 60, 230 (1975).
[19]M. S. Patterson, Proc. Phys. Soc. Lond. 63, 477 (1950).
[20]R. V. Southwell, *Relaxation Methods in Engineering Science* (Oxford U.P., London, 1946).
[21]J. M. Burkstrand, G. G. Kleiman, and F. J. Arlinghaus, Surf. Sci. 46, 43 (1974).
[22]J. E. Demuth and T. N. Rhodin, Surf. Sci. 42, 261 (1974).
[23]F. Jona, IBM J. Res. Develop. 14, 444 (1970).
[24]S. Wakoh, J. Phys. Soc. Jpn. 20, 1894 (1965).
[25]E. C. Snow, Phys. Rev. 158, 683 (1967).
[26]D. W. Jepsen, P. M. Marcus, and F. Jona, Phys. Rev. B 6, 3684 (1972).
[27]J. E. Demuth, P. M. Marcus, and D. W. Jepsen, Phys. Rev. B 11, 1460 (1975).
[28]C. J. Powell, Surf. Sci. 44, 29 (1974).